We are IntechOpen, the world's leading publisher of Open Access books
Built by scientists, for scientists

4,400
Open access books available

118,000
International authors and editors

130M
Downloads

Our authors are among the

154
Countries delivered to

TOP 1%
most cited scientists

12.2%
Contributors from top 500 universities

CLARIVATE ANALYTICS
BOOK CITATION INDEX
INDEXED

WEB OF SCIENCE™

Selection of our books indexed in the Book Citation Index
in Web of Science™ Core Collection (BKCI)

Interested in publishing with us?
Contact book.department@intechopen.com

Numbers displayed above are based on latest data collected.
For more information visit www.intechopen.com

Microscale Mechanics of Plug-and-Play In Vitro Cytoskeleton Networks

Shea N. Ricketts, Bekele Gurmessa and Rae M. Robertson-Anderson

Abstract

This chapter describes recent techniques that have been developed to reconstitute and characterize well-controlled, tunable networks of actin and microtubules outside of cells. It describes optical tweezers microrheology techniques to characterize the linear and nonlinear mechanics of these plug-and-play in vitro networks from the molecular-level to mesoscopic scales. It also details fluorescence microscopy and single-molecule tracking methods to determine macromolecular transport properties and stress propagation through cytoskeleton networks. Throughout the chapter the intriguing results that this body of work has revealed are highlighted—including how the macromolecular constituents of cytoskeleton networks map to their signature responses to stress or strain; and the elegant couplings between network structure, macromolecular mobility, and stress response that cytoskeleton networks exhibit.

Keywords: cytoskeleton, actin, microtubules, microrheology, optical tweezers, fluorescence, microscopy, in vitro

1. Introduction

The cell cytoskeleton is a complex and dynamic network of filamentous proteins that provides cells with structural and mechanical integrity while enabling key dynamic features such as cell motility, cytokinesis, apoptosis, and division [1, 2]. The cytoskeleton is able to perform these diverse functions by exhibiting a wide range of mechanical and structural properties that are tuned by the properties of, and interactions between, its constituent filamentous proteins: actin, microtubules, and intermediate filaments.

Due to the critical importance of understanding cytoskeleton mechanics and structure, over the past several decades numerous researchers from diverse disciplines have performed in vitro, in vivo, in silico, and theoretical studies aimed at elucidating this open problem [1–17]. This collective body of work has made great strides in understanding the molecular structure and properties of individual actin filaments and microtubules, the viscoelastic properties of simple in vitro networks of cytoskeletal filaments, and the role that various crosslinking proteins play in the resulting architecture and mechanical properties of actin networks. Complementary in vivo studies have focused on identifying key motifs that arise in different cell

types, in different regions of the cell, and during different phases in the cell cycle. These studies have demonstrated that the cytoskeleton can exhibit complex and nonlinear viscoelastic responses to strain; and that the lengths, concentrations and interactions between the comprising filaments play key roles in this response.

However, due to the diverse and complex mechanical responses and morphologies that cytoskeleton networks can exhibit, a connection between structure and mechanics in the cytoskeleton has proven elusive. The macromolecular properties and dynamics of the individual cytoskeleton filaments that give rise to the network stress response is also an open question. This chapter focuses on methods to overcome these issues including: the design of well-controlled in vitro cytoskeleton networks (Section 2), active microrheology methods to characterize the mechanical properties of these networks at the molecular and cellular scales (Section 3), and fluorescence microscopy techniques to measure network transport properties, mobility and structure (Section 4).

2. Preparation of tunable plug-and-play in vitro cytoskeleton networks

Over the past few decades, researchers have developed methods to create a range of cytoskeleton networks in vitro [3, 6, 11, 18–20]. Key issues that arise when creating and studying these networks are reproducibility and stability. There are also limited methods for creating networks comprised of multiple types of cytoskeleton filaments [6, 18]. Further, many of these systems exhibit structural and mechanical properties that vary from sample to sample, and exhibit aging and instability such that measurements are highly-dependent on the timescale of the measurement and age of the sample.

In vitro networks of semiflexible actin filaments have been most widely studied, spanning protein concentrations from the dilute to the nematic regimes, and incorporating numerous types of actin binding proteins (ABP) to create crosslinked and bundled networks [3, 13, 16, 19]. The motor protein, myosin II, has been used to create active and dynamic actin networks [4, 21, 22]. In vitro networks of rigid microtubules have also been studied, though less extensively [8, 14]. Far fewer studies have focused on composite networks of actin and microtubules, stemming from the incompatibility of established in vitro polymerization conditions for each protein. However, protocols have recently been developed to overcome this issue [18, 23].

Below are protocols to create highly stable, reproducible and tunable in vitro networks of actin and microtubules that mimic key biomimetic motifs and interactions. Further details regarding protocols can be found here [24]. These networks include actin networks with varying concentrations of crosslinkers, actin networks bundled by counterion condensation, and composite networks of sterically and chemically interacting actin filaments and microtubules. All networks are created by polymerization of actin monomers and/or tubulin dimers in an experimental sample chamber, rather than flowing in pre-formed filament networks, such that the native network structure and dynamics are preserved. To ensure reproducibility and stability, biotin-NeutrAvidin bonding and counterion condensation are used, rather than physiological ABPs, to create filament crosslinks and bundles.

2.1 Required buffers and reagents for networks described in Sections 2.2–2.4

PEM-100: 100 mM K-PIPES (pH 6.8), 2 mM EGTA, 2 mM $MgCl_2$. Store at room temperature (RT).

G-buffer: 2.0 mM Tris (pH 8), 0.2 mM ATP, 0.5 mM DTT, 0.1 mM $CaCl_2$. Store at −20°C.

10× F-buffer: 100 mM Imidazole (pH 7.0), 500 mM KCl, 10 mM MgCl$_2$, 10 mM EGTA, 2 mM ATP. Store at −20°C.

Oxygen scavenging system: 4.5 mg/mL glucose, 0.5% β-mercaptoethanol, 4.3 mg/mL glucose oxidase, 0.7 mg/mL catalase. Make fresh immediately prior to mixing into experimental sample. *Used to slow photobleaching during imaging when networks or microspheres have been fluorescent-labeled (see Section 4).*

1% (v/v) Tween: Used to prevent filaments from adsorbing to sample chamber surface. Dilute in working buffer.

100 mM GTP: Store at −20°C. Dilute to experimental concentration in PEM-100 and keep on ice.

100 mM ATP (pH to 7.0**)**: Store at −20°C. Dilute to experimental concentration in working buffer (PEM-100 or G-buffer) and keep on ice.

2 mM Taxol: Suspend 1 mg Pacilitaxol (Sigma, T7402) in DMSO. Store at −20°C.

PEM-Taxol: 198 µL PEM-100, 2 µL 2 mM Taxol. Make fresh for every sample. Store at RT.

200 µM Taxol: 18 µL DMSO, 2 µL 2 mM Taxol. Make fresh for every sample. Store at RT.

Tubulin (*T*, Cytoskeleton #T240): Resuspend to 5 mg/mL in PEM-100. Store in 5 µL aliquots at −80°C.

Biotinylated Tubulin (*B-T*, Cytoskeleton #T333P): Resuspend to 5 mg/mL in PEM-100. Store in 2 µL aliquots at −80°C.

Rhodamine Tubulin (*R-T*, Cytoskeleton #TL590): Prepare 5 mg/mL solutions of 1:10 molar ratio [Rhodamine tubulin]:[tubulin]. Store in 5 µL aliquots at −80°C.

Example: bring 20 µg R-tubulin to 5 mg/mL by adding 4 µL PEM-100. Add 36 µL of 5 mg/mL tubulin (T) to 4 µL R-tubulin.

Actin (*A*, Cytoskeleton, #AKL99): Resuspend lyophilized protein to 2 mg/mL in G-buffer. Store in 25 µL aliquots at −80°C.

Biotinylated actin (*B-A*, Cytoskeleton #AB07): Resuspend lyophilized protein to 1 mg/mL in G-buffer. Store in 5 µL aliquots at −80°C.

Alexa-568-actin (*5-A*, ThermoFisher #A12374): Dilute to 1.5 mg/mL in G-buffer. Store in 5 µL aliquots at −80°C.

Alexa-488-actin (*4-A*, ThermoFisher #A12373): Dilute to 1.5 mg/mL in G-buffer. Store in 5 µL aliquots at −80°C.

Biotin (*B*, Sigma #B4501): Resuspend to 102 mM in deionized water (DI) and store at 4°C.

NeutrAvidin (*NA*, ThermoFisher #31000): Resuspend to 5 mg/mL in PEM-100. Store in 5 µL aliquots at −20°C.

Experimental sample preparation: For all cytoskeleton networks described below, a volume V_F = 20 µL of protein monomers, reagents, and buffers are mixed together and quickly pipetted into a sample chamber constructed from a glass slide and a microscope coverslip separated by two layers of double-sided tape. Sample chambers are sealed with epoxy and incubated (time and temperature depend on network) to form networks of filamentous proteins.

2.2 Entangled and crosslinked actin networks

2.2.1 Entangled actin at any concentration c *(mg/mL) and final sample volume* V$_F$

$V_{PEM-100} = V_F − V_{Actin} − V_{ATP} − V_{Tween} − V_{OS}{}^*$
$V_{Actin} = (cV_F)/[A]$
$V_{ATP} = 0.1V_F$ 10 mM ATP
$V_{Tween} = 0.05V_F$ 1% Tween

V_{OS} = 0.05V_F oxygen scavenging system*
**If not imaging networks replace V_{OS} with PEM-100.*
Incubate at RT for 60 min.

Actin concentrations should be c = 0.1–2.5 mg/mL for entangled networks.

2.2.2 Pre-assembled biotin-NeutrAvidin crosslinker assay

To reproducibly form stable networks of crosslinked actin filaments that are isotropically crosslinked and free of bundling, it is important to pre-assemble Biotin-NeutrAvidin crosslinker complexes before adding to actin monomers to initiate network formation. Each complex is comprised of 1 NeutrAvidin (NA), 2 biotins (B), and 2 biotin-actin monomers (B-A). The molar ratio R of crosslinker to total actin [T-A] can be varied according to the following:
[T-A] = [A] + [B-A]; R = [N-A]/([T-A]); R = ½ [B-A]/([T-A]); [NA] = ½
[B-A] = ½[B]
Recipe for preparing crosslinker complexes that are concentrated by a factor X in a volume V_{FC}. Prepared complexes are viable for ~24 h on ice.

	Equations for a given R	**Ex. R = 0.07**
Concentration factor, X	2–20	4 µL
G-buffer volume	$V_{G-Buffer} = V_{FC} - V_{NA} - V_{B-A} - V_B$	2.4 µL
NeutrAvidin volume	$V_{NA} = X(V_{FC}R[T-A]/[NA])$	0.8 µL
Biotinylated actin volume	$V_{BA} = X(V_{FC}2R[T-A]/[B-A])$	5.6 µL
Biotin volume	$V_B = X(V_{FC}2R[T-A]/[B])$	1.2 µL

Sonicate complex solution for 90 min at 4°C.
Add volume V_{CL} to solution below.

2.2.3 Crosslinked network with any given R and [T-A]

$V_{G-buffer} = V_F - V_{Actin} - V_{CL} - V_{10xF} - V_{OS}$
$V_{Actin} = ([T-A]V_F)/[A]$
$V_{CL} = V_F/X$
$V_{10\times F} = 0.1V_F$ 10× F-buffer
$V_{OS} = 0.05V_{Final}$ Oxygen scavenging system*
**If not imaging networks replace V_{OS} with G-buffer.*

2.3 Reversibly bundled actin networks

Bundled actin networks are formed via counterion condensation using high concentrations of $MgCl_2$ and KCl. $MgCl_2$ concentrations of c_M > 4 mM will bundle actin when paired with KCl at a concentration of $2c_M$ (**Figure 1**).

Bundled actin network with actin concentration c (mg/mL) and $MgCl_2$ concentration c_M (mg/mL) in a final volume V_F
$V_{PEM-100} = V_F - V_{Actin} - V_{ATP} - V_{Tween} - V_{MgCl2} - V_{KCl} - V_{OS}$*
$V_{Actin} = cV_F/[A]$
$V_{ATP} = 0.1V_F$ 10 mM ATP
$V_{Tween} = 0.05V_F$ 1% Tween
$V_{MgCl2} = c_M V_F/[5 \text{ M } MgCl_2]$

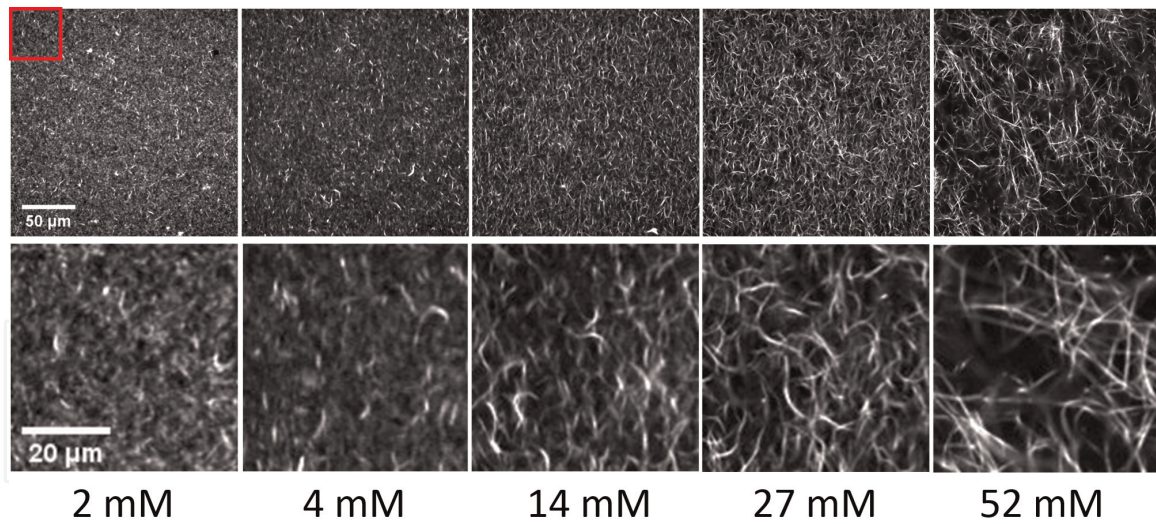**Figure 1.**
Confocal micrographs of actin networks (c = 5.8 μM) with varying degrees of bundling determined by the MgCl₂ concentration (listed below each image). Images shown are average intensity projections from 60 s time-series (4 fps) taken on a Nikon A1R laser scanning confocal microscope with 60× objective.

$$V_{KCl} = 2c_M V_F / [\text{4 M KCl}]$$
$$V_{OS} = 0.05 V_{Final} \text{ oxygen scavenging system}^*$$
If not imaging networks replace V_{OS} with PEM-100.

2.4 Composite networks of actin and microtubules

Co-entangled networks of actin and microtubules can be prepared with varying molar fractions of tubulin, $\phi_T = [tubulin]/([actin] + [tubulin])$, and total protein molarity, $[T\text{-}P] = [tubulin] + [actin]$. Composites are formed in PEM-100 with 1 mM ATP (for actin polymerization), 1 mM GTP (for tubulin polymerization) and 5 μM Taxol (for microtubule stabilization). To crosslink actin and/or microtubules within composites, biotin-NeutrAvidin complexes similar to those described in Section 2.2 can be prepared using either actin, tubulin, or both proteins (**Figure 2**).

2.4.1 Entangled actin-microtubule network with ϕ_T, [T-P] and final sample volume V_F

$$V_{PEM\text{-}100} = V_F - V_{Tubulin} - V_{Actin} - V_{GTP} - V_{ATP} - V_{Tween} - V_{Taxol} - V_{OS}^*$$
$$V_{Tubulin} = \phi_T [T\text{-}P] V_F / [T]$$
$$V_{Actin} = (1 - \phi_T)[T\text{-}P] V_F / [A]$$
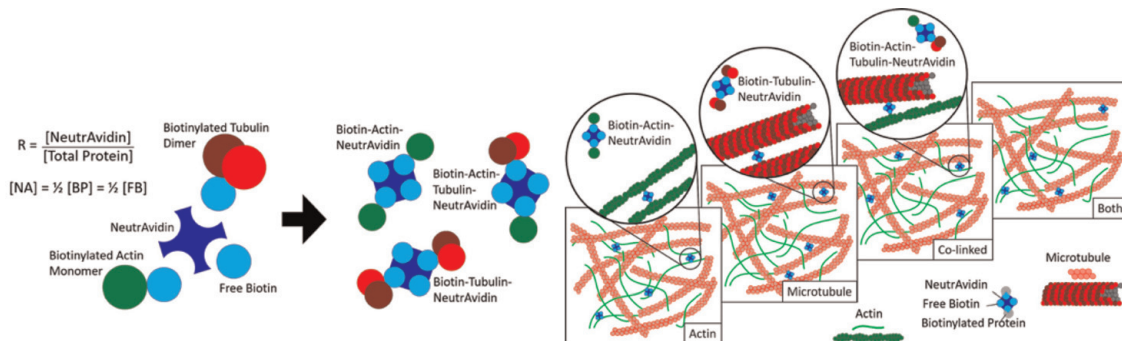$$V_{GTP} = 0.1 V_F \text{ 10 mM GTP}$$

Figure 2.
(Left) Biotin-NeutrAvidin crosslinkers. (Right) Actin-microtubule networks in which: actin is crosslinked (Actin), microtubules are crosslinked (Microtubule), actin and microtubules are linked to each other (Co-linked), both the actin network and microtubule network are crosslinked (Both).

$V_{ATP} = 0.1V_F$ 10 mM ATP
$V_{Tween} = 0.025V_F$ 1% Tween
$V_{Taxol} = 0.025V_F$ 200 μM Taxol (in DMSO)
$V_{OS} = 0.05V_F$ oxygen scavenging system*
If not imaging networks replace V_{OS} with PEM-100.
Incubate at 37°C for 60 min.

2.4.2 Recipe for preparing crosslinker complexes that are concentrated by a factor X in a volume V_{FC}

Prepared complexes are viable for ∼24 h on ice. Biotinylated protein [*B-P*] used depends on the type of crosslinking as follows:
Actin: [B-P] = [B-A]
Microtubule: [B-P] = [B-T]
Co-linked: [B-P] = [B-A] + [B-T]; [B-A] = [B-T] = ½[B-P]
Both: Prepare Actin and Microtubule solutions. Add equal parts of each to final sample chamber.

	Equations for a given R	Ex. R = 0.02
Concentration factor, X	Number ranging from 2 to 20	4 μL
PEM-100 volume	$V_{PEM-100} = V_{FC} - V_{NA} - V_{B-P} - V_B$	5.28μL
NeutrAvidin volume	$V_{NA} = X(V_{FC}R[T-P]/[NA])$	2.79μL
Biotinylated protein volume	$V_{BP} = X(V_{FC}2R[T-P]/[B-P])$	1.02μL
Biotin volume	$V_B = X(V_{FC}2R[T-P]/[B])$	0.91μL

Sonicate complex solution for 90 min at 4°C.
Add volume V_{CL} to solution below.

2.4.3 Crosslinked network for any given R, ϕ_T and total protein concentration, [T-P]

$V_{PEM-100} = V_F - V_{Tubulin} - V_{Actin} - V_{CL} - V_{GTP} - V_{ATP} - V_{Tween} - V_{Taxol} - V_{OS}$*
$V_{Tubulin} = (\phi_T[T-P]V_F)/([T] - 2R[T-P])$
$V_{Actin} = ((1-\phi_T)[T-P]V_F)/([A] - 2R[T-P])$
$V_{CL} = V_F/X$
$V_{GTP} = 0.1V_F$ 10 mM GTP
$V_{ATP} = 0.1V_F$ 10 mM ATP
$V_{Tween} = 0.025V_F$ 1% Tween
$V_{Taxol} = 0.025V_F$ 200 μM Taxol (in DMSO)
$V_{OS} = 0.05V_F$ oxygen scavenging system*
If not imaging networks replace V_{OS} with PEM-100.

3. Optical tweezers microrheology measurements

Given the importance of cytoskeleton mechanics to cell function, coupled with the complexity of mechanical properties that cells exhibit, understanding the response of cytoskeleton networks to stress and strain remains an important topic of research. Using standard bulk rheology techniques to measure the mechanical properties of cytoskeleton networks has been problematic due to the difficulty and expense in producing ∼mL sample volumes often needed for these measurements.

Further, these measurements probe the macroscopic mechanical properties of the networks but are unable to probe mechanics at the molecular and cellular scales (~μm). Finally, these methods are ill-equipped to measure spatial heterogeneities in network response, and can irreversibly disrupt or damage the network. Microrheology offers a complementary approach to characterizing the microscale mechanical and viscoelastic properties of cytoskeleton networks. While passive microrheology tracks freely diffusing microspheres embedded in networks to extract viscoelastic moduli, active microrheology uses optical tweezers to actively force embedded microspheres through networks and measure the force exerted to resist this strain. Active microrheology enables one to probe both molecular and mesoscopic scales and perturb networks far from equilibrium to access the nonlinear regime. Specifically, optical tweezers can be used to drag microspheres over distances that are large (5–30 μm) relative to the mesh size of the network (<μm) at speeds much faster than the molecular relaxation rates. The force exerted on the bead to resist the strain, as well as the subsequent relaxation of force following strain, is measured.

Reference [25] provides a thorough overview of the underlying principles and execution of optical tweezers microrheology to characterize the mechanics of bio-polymer networks. Here, the focus is on the key results obtained using the in vitro cytoskeleton networks described in Section 2 [18, 19, 26–28].

3.1 Entangled actin networks

Active microrheology experiments have been carried out on entangled actin networks (Section 2.1) to characterize the dependence of the viscoelastic response and stress relaxation on the rate of the applied microbead strain $\dot{\gamma}$ and actin concentration c (1 mg/mL = 23.2 μM) [26, 27]. The results are largely described within the framework of the tube model for entangled polymers, pioneered by de Gennes and Doi and Edwards [29, 30]. Comparisons to new theories and extensions of the tube model are also highlighted [31–33].

3.1.1 Strain rate dependence

Entangled actin networks (c = 0.5 mg/mL; mesh size ξ = 0.42 μm) subject to strain rates of $\dot{\gamma}$ = 1.4–9.4 s^{-1} (corresponding to speeds of v = 1.5–10 m/s) display a unique crossover to appreciable nonlinearity at a strain rate $\dot{\gamma}_c$ comparable to the theoretical rate of relaxation of individual entanglement segments τ_{ent}^{-1}. Above $\dot{\gamma}_c$, networks exhibit stress-stiffening, which, importantly, is not apparent at the macroscopic scale. This stiffening behavior occurs over very short time scales, comparable to the predicted timescale over which mesh size deformations relax τ_ξ, and has been shown to arise from suppressed filament bending. At times longer than τ_ξ, deformed entanglement segments are able to bend to release stress, and stress softening ensues until the network ultimately yields to an effectively viscous regime, over a timescale comparable to τ_{ent}. This terminal viscous regime exhibits shear thinning due to release of entanglements, with scaling $\eta \sim \dot{\gamma}^{-0.34}$, which is notably less pronounced than the thinning exhibited by flexible entangled polymers ($\eta \sim \dot{\gamma}^{-1}$). Surprisingly, the force relaxation following strain proceeds more quickly for increasing strain rates; and for rates greater than $\dot{\gamma}_c$, the relaxation displays a complex power-law dependence on time, as opposed to the expected exponential decay. This power-law relaxation is indicative of dynamic strain-induced entanglement tube dilation and healing, which corroborates recent theoretical predictions for rigid rods [31, 34].

3.1.2 Concentration dependence

These studies were extended to entangled actin networks of varying concentrations (c = 0.2–1.4 mg/mL) to reveal a previously unpredicted and unreported critical concentration c_c = 0.4 mg/mL for nonlinear response features to emerge. Beyond c_c, entangled actin stiffens for times below τ_ξ, with the degree of stiffening S and stiffening time scale t_{stiff} scaling inversely with the theoretical entanglement tube diameter d_t, i.e., $S \sim d_t^{-1} \sim c^{3/5}$. At longer times, the network yields to a viscous regime with the distance d_y and corresponding force f_y at which yielding occurs scaling inversely with the length between entanglements l_{ent} along each filament: $f_y \sim d_y \sim l_{ent}^{-1} \sim c^{2/5}$. Stiffening and yielding dynamics are consistent with recent predictions of nonlinear strain-induced breakdown of the cohesive entanglement force, which predicts the onset of yielding to occur when the induced force balances the cohesive elastic force provided by the entanglements [27, 32]. Following strain, the force relaxation displays distinct behaviors for $c > c_c$ versus $c < c_c$. For $c < c_c$, relaxation follows a single exponential decay with a decay time that scales according to tube model predictions for the disengagement time $\tau_D \sim c^{6/5}$. For $c > c_c$ relaxation proceeds via two distinct mechanisms: slow reptation out of dilated tubes with $\tau_{D'} \sim c^{1/5}$ coupled with $\sim$10$\times$ faster lateral hopping. Tube dilation and the commensurate reduction in reptation time $\tau_{D'}/\tau_D$ scales as c^{-1}, in agreement with recent predictions for entangled rigid rods [34, 35]. This model also predicts faster lateral hopping out of constraining tubes due to temporary fluctuation-induced yielding. The coupled emergence of lateral hopping with concentration-dependent dilation indicates that hopping only plays a significant role when entanglement tubes are sufficiently dilated to allow for fluctuation-induced transient yielding of tube constraints.

3.2 Crosslinked actin networks

As detailed in Section 2.2, methods have been developed to produce highly stable and reproducible networks of randomly-oriented crosslinked actin filaments. With these methods, the crosslinker density can be systematically tuned while fixing the actin concentration and structural network properties (i.e., isotropic filament orientation, no bundling).

Nonlinear microrheological characterization of these networks have been carried out for crosslinking ratios of R = 0–0.07 (c = 0.5 mg/mL) [19]. For all R values, networks exhibit initial stiffening due to entropic stretching of filaments along the strain path, followed by stress softening and yielding to a steady-state regime. The maximum stiffness achieved K_{max} as well as the time to yield to the terminal regime scale exponentially with R. The critical decay constant associated with this scaling, $R^* \sim 0.014$, corresponds to a crosslinker length l_c equal to the theoretical entanglement length l_e. Networks with higher R values also exhibit more sustained elastic resistance in the terminal regime such that the terminal stiffness K_t scales exponentially with R with a similar critical ratio $R^* \sim 0.018$. These stress response characteristics suggest that softening and yielding arise from force-induced disentanglement and crosslinker unbinding while crosslinker rebinding events allow for the observed sustained terminal elasticity.

Following strain, all networks exhibit exponential force decay with two distinct timescales. Similar to the stress response characteristics, both fast and slow relaxation times scale exponentially with R with comparable R^* values of ~ 0.008, which likewise corresponds to $l_c \sim l_e$. For $R > R^*$ networks are able to maintain high levels of elastic stress following the strain, which is quantified by the terminal force value F_t at the end of the 30 s relaxation phase. Once again, $F_t \sim e^{R/R^*}$ with $R^* \sim 0.007$. As

further discussed in Section 4.3, this long-lived post-strain stress is likely a result of the network distributing stress to a small fraction of highly strained connected filaments that span the network, allowing the rest of the network to relax [28].

These intriguing results, along with the corresponding actin filament deformations and stress propagation dynamics that lead to the force response, are further explored in Section 4.3.

3.3 Co-entangled composite networks of actin and microtubules

As described in Section 2.4, techniques have recently been developed to create randomly oriented, co-entangled networks of actin and microtubules by simultaneously co-polymerizing varying ratios of actin and tubulin in situ. The relative concentrations of actin and microtubules, quantified by the molar fraction of tubulin ϕ_T, as well as the overall protein concentration $[T\text{-}P]$, can be systematically varied over a wide range of values while maintaining composite integrity and stability. Different crosslinking interactions and motifs can also be methodically introduced and tuned.

Seminal microrheology studies on these composites have been carried out for ϕ_T values of 0 to 1 with $[T\text{-}P]$ held fixed at 11.6 μM [18, 23]. These studies show that composites comprised of mostly actin ($\phi_T < 0.5$) initially exert a $\sim100\times$ higher resistive force in response to strain, compared to networks comprised of mostly microtubules ($\phi_T > 0.5$). However, the rise in force with strain distance is steeper for $\phi_T > 0.5$ networks such that at ~5 μm, the force became larger for $\phi_T > 0.5$ composites compared to $\phi_T < 0.5$. Actin-rich composites are also initially relatively stiff but quickly softened, whereas microtubule-rich composites display an initially soft/viscous response followed quickly by stiffening such that at the end of the strain the stiffness for $\phi_T > 0.5$ networks was $\sim10\times$ higher than their actin-rich counterparts. The initial force response can be understood in terms of poroelastic models, which consider the dynamics of the mesh as well as the pervading fluid [14, 36]. In these models, the faster the timescale for water to drain from the deformed mesh (τ_p), the faster the system can relax, such that it will exert a concomitantly smaller initial force on the bead. The poroelastic timescale, which depends both on the elastic modulus and mesh size of the network, is $\sim40\times$ longer for actin networks than for microtubule networks [18], resulting in a comparably higher initial force and stiffness for actin-rich composites versus microtubule-rich composites. The subsequent sharp transition from softening to stiffening when ϕ_T exceeds 0.5, arises from microtubules suppressing actin bending fluctuations.

The presence of a large fraction of microtubules ($\phi_T > 0.7$) result in large heterogeneities in force response as well as increased average resistive force. Heterogeneities arise from the increasing mesh size of the composite as ϕ_T increases, as well as more frequent microtubule buckling events. As ϕ_T increases the mesh size of the composite increases from $\xi_A \sim 0.42$ μm for $\phi_T = 0$ to $\xi_M \sim 0.89$ μm for $\phi_T = 1$. Thus, at the microscale, the system becomes increasingly more heterogeneous as ϕ_T increases. Further, for a composite with equal molar fractions of actin and microtubules ($\phi_T = 0.5$), the mesh size of the microtubule network is $\sim2\times$ that of the actin network ($\xi_A \sim 2\xi_M$), and the actin mesh remains smaller than the microtubule mesh until $\phi_T > 0.7$. Thus, actin network characteristics dominate the force response until relatively large fractions of microtubules are incorporated. This effect, combined with force-induced buckling of microtubules to alleviate stress, leads to a nonlinear increase in resistive force as ϕ_T increases.

Force relaxation following strain exhibits two-phase power-law decay with the first decay arising from actin bending modes while the long-time relaxation is indicative of filaments reptating out of deformed entanglement constraints.

Interestingly, the scaling exponents for the long-time relaxation exhibits a non-monotonic dependence on ϕ_T, reaching a maximum for equimolar composites (ϕ_T = 0.5), which suggests that filament diffusion (i.e., reptation) is fastest at ϕ_T = 0.5. This non-monotonic trend likely arises from a competition between increasing mesh size as ϕ_T increases, which increases filament mobility, versus increasing filament rigidity (replacing actin with microtubules), which suppresses filament mobility. See Section 4.2 for more discussion of this result.

4. Fluorescence imaging and characterization of network transport, mobility and structure

A key question regarding the cytoskeleton is how the mechanical force response couples to both network structure as well as the mobility and deformations of the comprising filaments. To address this problem, a range of fluorescence labeling schemes can be incorporated into in vitro networks, and various microscopy methods can be employed to image networks and quantify mobility and structure. This section describes different in vitro labeling and imaging methods as well as key results and parameters that can be obtained with the described methods.

4.1 Fluorescence labeling of proteins for varied measurement methods

Below are protocols for three different labeling schemes optimized for different network characterizations and imaging methods: (1) doping networks with pre-formed labeled filaments [18, 27], (2) in situ network labeling [23], and (3) labeling discrete filament segments for particle-tracking [19, 28].

4.1.1 Doping networks with pre-formed labeled filaments

This method is ideal for measuring filament length distributions and resolving single-filament fluctuations and mobility (**Figure 3**).
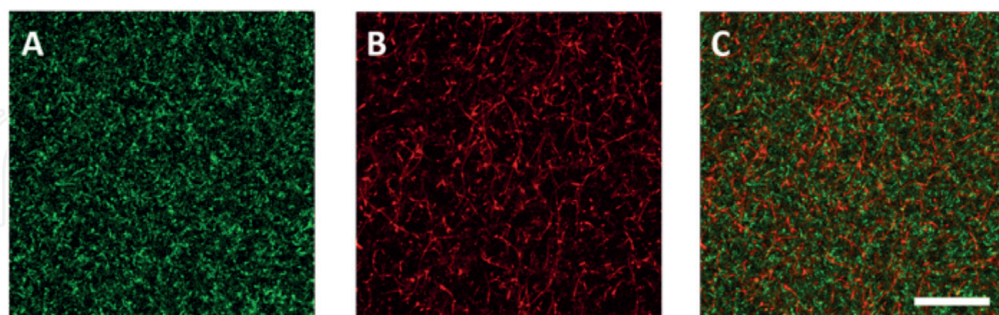

Figure 3.
Two-color laser scanning confocal imaging of fluorescent-labeled equimolar actin-microtubule composite ([T-P] = 11.6 μM). (A) The actin (green) channel, (B) microtubule (red) channel and (C) both channels show actin filaments and microtubules within composites form networks that overlap with each other forming a homogeneous network with no phase separation or clustering. The scale bar is 50 μm and applies to all images. The 512 × 512 image is taken on a Nikon A1R laser scanning confocal microscope with a 60× objective and QImaging CCD camera.

4.1.1.1 Labeled actin filaments for actin networks (Sections 2.2 and 2.3)

Prepare 10 μL of a 5 μM solution of 1:1 [5-A]:[A] to polymerize prior to adding to actin network:
    7.75 μL G-buffer

0.72 μL 5-A
0.54 μL A
1 μL 10× F-buffer

Incubate for 60 min at RT.
Prepare a 1:2 dilution in PEM-100 or F-buffer (depending on desired final buffer).
Add 1 μL of dilution to final sample chamber solution from Section 2.2 or 2.3, replacing the equivalent volume of PEM-100 or G-buffer (depending on network).

4.1.1.2 Labeled filaments for actin-microtubule composites (Section 2.4)

Alexa-488-actin filaments
Prepare 10 μL of a 5 μM solution of 1:1 [4-A]:[A] to polymerize prior to adding to composite:
6.74 μL PEM-100
0.72 μL 4-A
0.54 μL A
2.00 μL 10 mM ATP

Incubate for 60 min at RT.
Immediately prior to imaging prepare a 1:2 dilution in PEM-100 + 2 mM ATP.
Add 1 μL to final sample chamber solution from Section 2.4, replacing the equivalent volume of PEM-100.

Rhodamine-labeled microtubules
Prepare 5 μL of a 37 μM solution of R-T to polymerize prior to adding to composite as follows:
Thaw R-T aliquot in hand.
Add 0.55 μL 10 mM GTP.
Incubate at 37°C for 30 min.
Add 0.6 μL of 200 μM Taxol.
Incubate at 37°C for 30 min.
Immediately prior to imaging prepare a 1:10 dilution in PEM-Taxol.
Add 1 μL to final sample chamber solution from Section 2.4, replacing the equivalent volume of PEM-100.
Labeled filaments can be stored at RT for up to 1 week. After day 1, shear microtubules with a sterile hamilton syringe before adding to the sample chamber.

4.1.2 In situ network labeling

In this method labeled monomers are added to solution prior to in situ network formation, rather than adding pre-formed filaments [23]. This method, demonstrated in **Figures 1** and **4** provides the most accurate depiction of network architecture and enables evaluation of network formation during polymerization. The drawback is that rarely are discrete single filaments visible, preventing filament length measurements. The ratio of labeled (4-A, 5-A or R-T) to unlabeled (A or T) monomers can range from 1:50 to 1:5 depending on the overall protein concentration and type of fluorescent dye used. Below are recipes for optimized samples of entangled actin and actin-microtubule composites.

4.1.2.1 Example of in situ labeled actin network

c = 1 mg/mL, [5-A]:[A] = 1:9.6, V_F = 20 μL
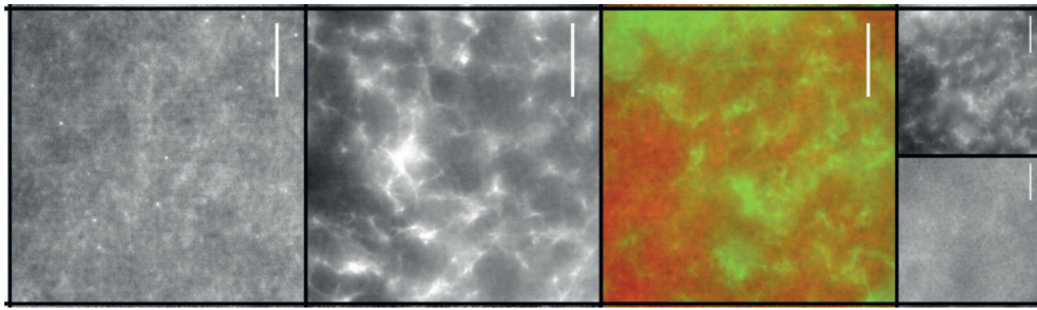
6.3 μL PEM-100

Figure 4.
Epifluorescence imaging of in situ labeling of an actin network (left), microtubule network (middle), and equimolar actin-microtubule composite (right). Images are sum projections of 400-frame time series (40 fps) taken using an Olympus IX73 microscope with 60× objective. The composite image also shows the separate channels for microtubules (top, far right) and actin (bottom, far right). All scale bars represent 10 μm.

1.2 μL 5-A
9.1 μL A
0.4 μL 100 μM ATP
1 μL 1% Tween
2 μL oxygen scavenging system.

4.1.2.2 Example of in situ labeled actin-microtubule composite

$[T\text{-}P]$ = 11.6 μM, ϕ_T = 0.5, $[4\text{-}A]$:$[A]$ = 1:4.8, $[R\text{-}T]$:$[T]$ = 1:35.7, V_F = 20 μL

3.43 μL PEM-100
0.29 μL 4-A
1.03 μL A
0.83 μL R-T
0.87 μL T
1 μL 10 mM ATP
1 μL 10 mM GTP
0.5 μL 200 μM Taxol
0.5 μL 1% Tween
1 μL oxygen scavenging system

4.1.3 Labeling discrete filament segments for particle-tracking

Because actin and microtubules are extended filaments, standard particle-tracking methods, optimized for punctile objects, cannot be used. To overcome this limitation, one can generate actin filaments with discrete, well-separated labeled segments (**Figure 5**) through a multi-stage polymerization process that includes shearing and annealing of labeled actin segments. Below is the protocol to create discrete-labeled actin filaments.

Follow protocol in Section 4.1.1.1 to prepare pre-formed Alexa-568-labeled actin filaments.

Shear filaments with a 26 gauge Hamilton syringe 15 times.

Quickly add 1 μL of 2 mg/mL actin (*A*) and mix by pipetting 5 times. Incubate at RT for 20 min to allow labeled and unlabeled segments to anneal.

Prepare a 1:20 dilution in F-buffer. Mix by pipetting 5 times.

Add to final sample solution from Section 2.2 at a volume of $0.05V_F$, replacing the equivalent volume of PEM-100.
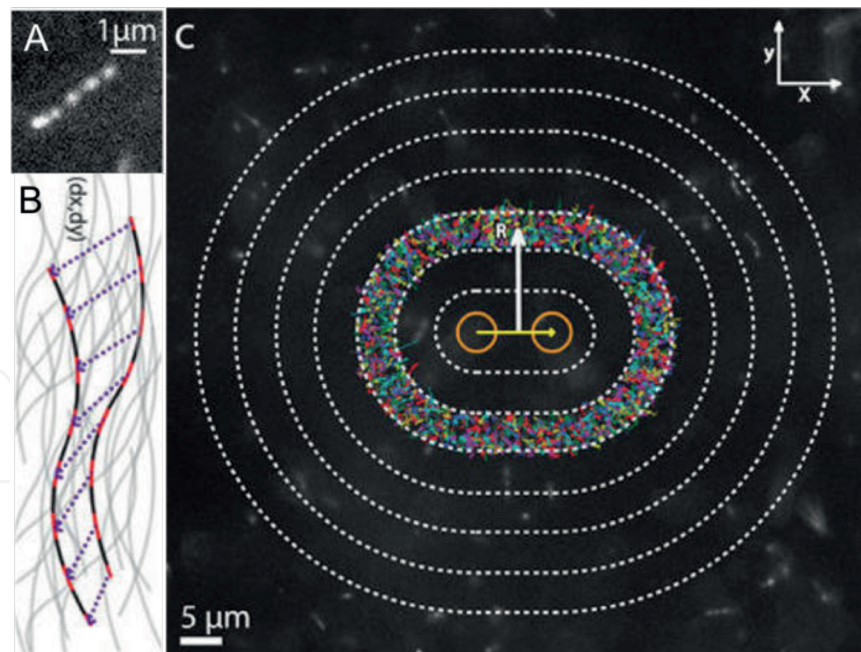
Figure 5.
Discrete labeling of actin filament segments for particle-tracking. (A) Microscope image of filament with interspersed ∼0.45 μm labeled segments that can be centroid-tracked during experiments. (B) Cartoon of tracking labeled segments along an actin filament. (C) Tracking discrete segments at varying distances R from strain path during microrheology experiments described in Section 3. Orange circles represent bead position before/after strain and yellow line represents strain path. Dotted lines outline annuli positioned every 4.5 μm from strain path (R = 6.75, 11.25, …, 29.25 μm). All tracks within each annulus are used to determine R dependence of strain-induced actin mobility.

4.2 Fluorescence confocal microscopy methods

Two-color fluorescence confocal microscopy allows for characterization of the 3D structure and mobility of networks comprised of multiple species (i.e., actin and microtubules). Use labeling method (1), the lengths, orientations, and mobility of single filaments within cytoskeleton composites can be resolved.

This method has been used to quantify the mobility of actin and microtubules within composites as described in Ref. [18]. Briefly, the standard deviation in pixel intensities over time can be computed from high frame-rate time-series and used to quantify the mobility of each filament type. Using this method, Reference [18] showed that the mobility of both actin and microtubules in co-entangled composites is greatest in equimolar composites (ϕ_T = 0.5). This surprising result, which aligns with the post-strain relaxation behavior (described in Section 3.3), arises from an interplay between varying mesh sizes and filament rigidity. Namely, as the fraction of microtubules in composites increases so does the mesh size, allowing for larger voids for filaments to move through (increasing mobility). However, increasing ϕ_T eventually comes at a cost as the majority of filaments are rigid rods rather than semiflexible filaments, which hinders bending modes and fluctuations and ultimately reduces mobility.

3D stacks of images can also be used to determine network structure and connectivity. Evaluating these types of images has shown that the actin and microtubule networks comprising composites are isotropic, entangled, and well-integrated with one another.

More recently developed in situ labeling methods (Section 4.1.2) can more accurately depict network architecture [23] and can be analyzed to determine network correlation lengthscales and fluctuation rates.

4.3 Molecular-tracking microrheology

To directly track filament motion during and following strain, one can incorporate labeling technique (3) into cytoskeleton networks. This method results in punctile segments along filaments that can be tracked over time to determine filament trajectories. Incorporating fluorescence imaging and particle-tracking algorithms into an optical tweezers setup allows for imaging of these segments during micorheology measurements [19, 28].

This method has been used to couple filament deformations and strain propagation to force response in entangled and crosslinked networks of actin [19, 28]. One key result of this work was to determine the origin of stress stiffening and softening in crosslinked actin networks (see Section 3.2). In particular, these studies showed that initial stiffening arises from acceleration of strained filaments due to molecular extension along the strain path, while softening and yielding is coupled to filament deceleration, halting, and recoil. Networks also display a surprising non-monotonic dependence of filament deformation on crosslinker concentration. Namely, networks with no crosslinks or substantial crosslinks both exhibit fast initial filament velocities and reduced molecular recoil while intermediate crosslinker concentrations display reduced velocities and increased recoil. These collective results arise from a balance of network elasticity and force-induced crosslinker unbinding and rebinding. In accord with recent simulations [28], this work also showed that post-strain stress can be long-lived in crosslinked networks by distributing stress to a small fraction of highly strained connected filaments that span the network and sustain the load, while the rest of the network is able to recoil and relax.

5. Conclusions

As described in the preceding sections, several recent advances in in vitro network design and microrheological measurement techniques have enabled key insights into the mechanics and mobility of cytoskeleton networks.

The engineered networks include actin and microtubule networks with well-defined, versatile crosslinking motifs; networks of actin bundles mediated by counterion crossbridges, and composite networks of sterically and chemically interacting actin filaments and microtubules. The protocols and design schemes for these networks are highly modular to facilitate introducing higher levels of complexity and expanding the phase space of molecular constituents and structures. The versatile fluorescence labeling and imaging methods described allow for robust characterization of network dynamics and structure, while the active microrheology studies described can characterize the linear and nonlinear mechanical properties of these networks at the molecular and cellular scales. Some of the key findings this body of work has revealed include: the existence of critical strain rates and concentrations for actin networks to exhibit nonlinear mechanics, the inhomogeneous nature of stress propagation throughout crosslinked actin networks, the important role that actin plays in suppressing the buckling of microtubules, and the elegant competition between mesh size and polymer stiffness that leads to emergent dynamics in actin-microtubule networks.

While many open questions remain, these presented advances open the door for a wide range of highly-controlled new experiments to explore the vast phase space of mechanical and structural properties of diverse cytoskeleton networks.

Acknowledgements

Conflict of interest

Authors declare no conflict of interest.

Author details

Shea N. Ricketts, Bekele Gurmessa and Rae M. Robertson-Anderson*
Department of Physics and Biophysics, University of San Diego, San Diego, California, United States

*Address all correspondence to: randerson@sandiego.edu

IntechOpen

References

[1] Pollard TD. The cytoskeleton, cellular motility and the reductionist agenda. Nature. 2003;**422**:741-745

[2] Gardel ML, Kasza KE, Brangwynne CP, Liu J, Weitz DA. Mechanical response of cytoskeletal networks. Methods in Cell Biology. 2008;**89**: 487-519

[3] Gardel ML, Shin JH, MacKintosh FC, Mahadevan L, Matsudaira P, Weitz DA. Elastic behavior of cross-linked and bundled actin networks. Science. 2004; **304**:1301

[4] Murrell MP, Gardel ML. F-actin buckling coordinates contractility and severing in a biomimetic actomyosin cortex. PNAS. 2012;**109**:20820-20825

[5] Dogterom M, Koenderink GH. Actin-microtubule crosstalk in cell biology. Nature Reviews Molecular Cell Biology. 2019;**20**:38-54

[6] Preciado López M, Huber F, Grigoriev I, Steinmetz MO, Akhmanova A, Dogterom M, et al. In vitro reconstitution of dynamic microtubules interacting with actin filament networks. Methods in Enzymology. 2014;**540**:301-320

[7] Fletcher DA, Mullins RD. Cell mechanics and the cytoskeleton. Nature. 2010;**463**:485-492

[8] Hoffman BD, Crocker JC. Cell mechanics: Dissecting the physical responses of cells to force. Annual Review of Biomedical Engineering. 2009;**11**:259-288

[9] Jensen MH, Morris EJ, Weitz DA. Mechanics and dynamics of reconstituted cytoskeletal systems. Biochimica et Biophysica Acta (BBA)—Molecular Cell Research. 2015;**1853**: 3038-3042

[10] Huber F, Boire A, López MP, Koenderink GH. Cytoskeletal crosstalk: When three different personalities team up. Current Opinion in Cell Biology. 2015;**32**:39-47

[11] Hawkins T, Mirigian M, Selcuk Yasar M, Ross JL. Mechanics of microtubules. Journal of Biomechanics. 2010;**43**:23-30

[12] Yang Y, Bai M, Klug WS, Levine AJ, Valentine MT. Microrheology of highly crosslinked microtubule networks is dominated by force-induced crosslinker unbinding. Soft Matter. 2012;**9**:383-393

[13] Gardel ML, Nakamura F, Hartwig J, Crocker JC, Stossel TP, Weitz DA. Stress-dependent elasticity of composite actin networks as a model for cell behavior. Physical Review Letters. 2006;**96**:088102

[14] Moeendarbary E, Valon L, Fritzsche M, Harris AR, Moulding DA, Thrasher AJ, et al. The cytoplasm of living cells behaves as a poroelastic material. Nature Materials. 2013;**12**:253-261

[15] Tsuda Y, Yasutake H, Ishijima A, Yanagida T. Torsional rigidity of single actin filaments and actin–actin bond breaking force under torsion measured directly by in vitro micromanipulation. PNAS. 1996;**93**:12937-12942

[16] Strehle D, Schnauß J, Heussinger C, Alvarado J, Bathe M, Käs J, et al. Transiently crosslinked F-actin bundles. European Biophysics Journal. 2011;**40**: 93-101

[17] Kim T, Gardel ML, Munro E. Determinants of fluidlike behavior and effective viscosity in cross-linked actin networks. Biophysical Journal. 2014; **106**:526-534

[18] Ricketts SN, Ross JL, Robertson-Anderson RM. Co-entangled

actin-microtubule composites exhibit tunable stiffness and power-law stress relaxation. Biophysical Journal. 2018; **115**:1055-1067

[19] Gurmessa B, Ricketts S, Robertson-Anderson RM. Nonlinear actin deformations lead to network stiffening, yielding, and nonuniform stress propagation. Biophysical Journal. 2017; **113**:1540-1550

[20] Gurmessa BJ, Bitten N, Nguyen DT, Saleh OA, Ross JL, Das M, et al. Triggered disassembly and reassembly of actin networks induces rigidity phase transitions. Soft Matter. 2018. 2019;**15**: 1335-1344. DOI: 10.1039/C8SM01912F.

[21] MS e S, Depken M, Stuhrmann B, Korsten M, MacKintosh FC, Koenderink GH. Active multistage coarsening of actin networks driven by myosin motors. PNAS. 2011;**108**:9408-9413

[22] Mizuno D, Tardin C, Schmidt CF, MacKintosh FC. Nonequilibrium mechanics of active cytoskeletal networks. Science. 2007;**315**:370-373

[23] Regan K, Wulstein D, Rasmussen H, McGorty R, Robertson-Anderson RM. Bridging the spatiotemporal scales of macromolecular transport in crowded biomimetic systems. Soft Matter. 2018. 2019;**15**:1200-1209. DOI: 10.1039/C8SM02023J

[24] https://docs.google.com/document/d/1QfCAac1OFhBnF-D9IZc7NvSnrUJNXwsm-ZuVjZKJDfI/edit?usp=sharing

[25] Robertson-Anderson RM. Optical tweezers microrheology: From the basics to advanced techniques and applications. ACS Macro Letters. 2018;**7**: 968-975

[26] Falzone TT, Blair S, Robertson-Anderson RM. Entangled F-actin displays a unique crossover to microscale nonlinearity dominated by entanglement segment dynamics. Soft Matter. 2015;**11**:4418-4423

[27] Gurmessa B, Fitzpatrick R, Falzone TT, Robertson-Anderson RM. Entanglement density tunes microscale nonlinear response of entangled actin. Macromolecules. 2016;**49**:3948-3955

[28] Falzone TT, Robertson-Anderson RM. Active entanglement-tracking microrheology directly couples macromolecular deformations to nonlinear microscale force response of entangled actin. ACS Macro Letters. 2015;**4**:1194-1199

[29] de Gennes P-G, Gennes PP-G. Scaling Concepts in Polymer Physics. Ithaca, NY: Cornell University Press; 1979

[30] Doi M, Edwards SF. The Theory of Polymer Dynamics. Oxford, UK: Clarendon Press; 1988

[31] Sussman DM, Schweizer KS. Microscopic theory of the tube confinement potential for liquids of topologically entangled rigid macromolecules. Physical Review Letters. 2011;**107**:078102

[32] Wang S-Q, Ravindranath S, Wang Y, Boukany P. New theoretical considerations in polymer rheology: Elastic breakdown of chain entanglement network. The Journal of Chemical Physics. 2007;**127**:064903

[33] Sussman DM, Schweizer KS. Entangled polymer chain melts: Orientation and deformation dependent tube confinement and interchain entanglement elasticity. The Journal of Chemical Physics. 2013;**139**:234904

[34] Sussman DM, Schweizer KS. Entangled rigid macromolecules under continuous Startup shear deformation: Consequences of a microscopically anharmonic confining tube. Macromolecules. 2013;**46**:5684-5693

[35] Sussman DM, Schweizer KS. Microscopic theory of quiescent and deformed topologically entangled rod solutions: General formulation and relaxation after nonlinear step strain. Macromolecules. 2012;**45**:3270-3284

[36] Kalcioglu ZI, Mahmoodian R, Hu Y, Suo Z, Van Vliet KJ. From macro- to microscale poroelastic characterization of polymeric hydrogels via indentation. Soft Matter. 2012;**8**:3393